https://doi.org/10.18321/ectj1436

Perovskite-Based Solar Cells: Some Problems and Ways of their Solution

N. Ashurov[1], B. Oksengendler[1], S. Maksimov[1,2], A. Zakhidov[3], G. Yar-Mukhamedova[4*], G. Zhamanbayeva[4,5]

[1]Institute of Polymer Chemistry and Physics, Academy of Sciences of the Republic of Uzbekistan, A. Kadyri Str., 7b, Tashkent, Uzbekistan
[2]Institute of Ion Plasma and Laser Technologies, Academy of Sciences of the Republic of Uzbekistan, Do'rmon Yo'li Str., 33, Tashkent, Uzbekistan
[3]University of Texas at Dallas, 800 West Campbell Road, Richardson, TX 75080-3021, USA
[4]Institute of Experimental and Theoretical Physics of Al-Farabi Kazakh National University, Al-Farabi ave., 71, Almaty, Kazakhstan
[5]Research Centre "KazAlfaTech LTD", Karasu str., 41A, Almaty, Kazakhstan

Article info

Received:
16 February 2022

Received in revised form:
28 March 2022

Accepted:
5 May 2022

Keywords:
Solar cells, Perovskite, Precursor solution, Nanoparticle shape

Abstract

The fundamental aspects of the perovskite absorber formation of solar irradiation for two generally accepted one- and two-step technologies are considered. For the on-step variant, two stages of perovskite formation, called "through solution" and "intermediate colloid compounds of precursors", were identified. The successive deposition of precursors is described in terms of thermodynamics and the Ostwald ripening model. The optimal conditions for the concentration and temperature for the spinning solution of methylammonium iodide to obtain various sizes of perovskite crystallites are presented. Examples are given for some other approaches that are used in the formation of high-quality perovskite films with high optoelectronic characteristics for a conversion rate of perovskite based solar cells on them.

1. Introduction

The search and study of materials that are promising from the point of view of their use in the developed efficient solar energy converters is the most important problem in modern alternative energy. The particular interest in recent years is connected with the creation of photovoltaic solar cells (SC) based on organic-inorganic perovskites [1–5]. Perovskites with an ABX_3 structure, where A is the organic part, B is metals (Pb, Sn, Cd, etc.), X is halogens (iodine, chlorine, bromine) [6–8], are the best representatives of the active layer in the third SC generation due to their excellent optoelectronic properties. These materials have high absorption coefficient, balanced charge-transport properties with long diffusion length and are very perspective for their manufacturability due to their low cost. Recent investigations have focused on improving the coverage, uniformity and morphology of the perovskite light absorber in frameworks of the different types of creation processes: one-step [9–11], two-step solution process [12–14], vapor process [15, 16], hybrid chemical vapor deposition (HCVD) [17], solvent annealing, mixed solutions and anti-solvent treatment [18–20], using co-solvent as a complexing and wetting agent for obtaining the high surface coverage and pinhole-free structure [21], cryo-controlled techniques [22]. These approaches allow controlling of the dynamics of nucleation and grain growth of $CH_3NH_3PbI_3$, crystallite sizes and crystallinity degree, ensuring the formation of extremely uniform and dense perovskite layers via a CH_3NH_3I-PbI_2-DMSO intermediate phase, which gives the certified power-conversion efficiency up to 16%. Among them two-step solution process is considered to be the most promising.

The excellent rapid growth of power conversion efficiency (PCE) of solar radiation into

*Corresponding author.
E-mail addresses: gulmira-alma-ata@mail.ru

© 2022 The Author(s). Published by al-Farabi Kazakh National University.
This is an open access article under the CC BY license (http://creativecommons.org/licenses/by/4.0/).

electrical energy from 3.8% in 2009 [23] to more as 25% [24, 25] in the perovskite-based SC has been achieved. Such achievements are based on the developed principles of the choice of absorber and electron (n) and hole (p) conductive components of the cell.

2. Basic types of perovskite solar cells

Based on the design features, there are two types of perovskite solar cells: mesoporous and planar. In turn, in terms of the sequence of working layers (to incident solar radiation), perovskite based SCs with n-i-p and p-i-n architecture are distinguished, respectively. So, three basic different types of perovskite SC configurations are presented. The first type with n-i-p structure has been made on nanocrystalline TiO_2 and could be called "regular mesoscopic structure". The most efficient SCs (~ 20% (see [26, 27]) are very thin (~ 150 nm) mesoporous TiO_2 scaffold. In such a configuration, n-type selective contact (normally compact TiO_2) is located in the bottom and the photo-generated electrons are collected by the front transparent conducting glass, usually indium tin oxide (ITO) or fluorine-doped tin oxide (FTO). The second type has a regular planar n-i-p structure; here the current flow direction is the same as in the first type, but without the mesoporous TiO_2 scaffold for electron collection. This cell configuration has a conversion efficiency of more than 19% [28]. A sample of this structure type has been presented in [29], where an insulated mesoporous Al_2O_3 scaffold has no evident electrical function in SC device. The third type of SC is a so-called "inverted planar" p-i-n- structure, where a compact p-type conducting layer is placed in the cell bottom. In this cell configuration, the photo-generated holes are collected by front conducting glass. Organic PEDOT:PSS (Poly(3,4-ethyllenedioxythiophene): Polystyrene sulfonate) [30–32] or inorganic NiO_x [33–40] are used as a hole conducting material. The cells of this configuration have small hysteresis.

3. Some features of the two-steps process of cell formation

Let us consider the features of one-step and two-step solution processes separately (Fig. 1) [41]. In the two-step process, the methylammonium iodide (MAI) solution is spin coated onto the pre-deposited PbI_2 film and then dried at 100 °C to form the perovskite phase. One-step and two-step spin-coating procedure for $CH_3NH_3PbI_3$ formation PbI_2 was mixed with CH_3NH_3I in *N,N*-dimethylacetamide (DMA), which was spin-coated and heated for one-step coating. For two-step coating, a PbI_2-dissolved *N,N*-dimethylformamide (DMF) solution was first spin-coated on the substrate, dried and then a CH_3NH_3I-dissolved isopropyl alcohol (IPA) solution was spin-coated on the PbI_2 coated substrate.

This process, however, has inherent drawbacks associated with the presence of unreacted lead iodide and voids due to the uneven distribution of perovskite crystallites, i.e., insufficient coverage of the substrate by the absorber. This phenomenon is a reason for the low reproducibility of the conversion of cells, which is especially pronounced for their planar configuration. Therefore, all the efforts of researchers are aimed at establishing a mechanism of the perovskite layer formation to achieve high optoelectronic characteristics of the solar absorber. From this point of view, the most important step is the reaction of the methylammonium iodide on the previously formed film of lead iodide, since from this moment the reaction between lead iodide and methylammonium iodide begins with the formation of the perovskite [42]:

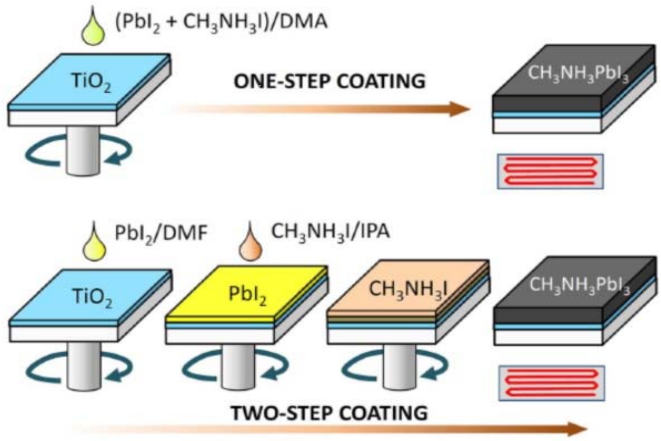

Fig. 1. Comparison of one-step and two-step solution processes. Source: Reprinted with kind permission [41].

$$PbI_2 + CH_3NH_3I \rightarrow MAPbI_3 \quad (1)$$

$$MAPbI_3 + I^- \underset{grows}{\overset{dissociation}{\rightleftharpoons}} CH_3NH_3 + PbI_4^{2-} \quad (2)$$

For the above reactions, it should be noted that lead iodide is not soluble in isopropanol (solvent for methylammonium iodide), however, the formed perovskite nuclei are susceptible to decomposition. Based on general considerations and experimental data it was revealed that the density of the nuclei is related to the concentration of methylammonium iodide in isopropanol and the morphology of the surface of the lead iodide film. According to the Ostwald ripening model [42], the coarsening of particles in a liquid medium is due to the material transport from small particles to large ones. As a rule, the concentration of dissolved particles near small particles is always greater than that near the surface of large particles, which ultimately leads to the appearance of the concentration gradient of dissolved particles. This situation is well described by Fick's law, namely, the transport of dissolved components from small to large particles is observed. Such a picture is quite applicable to the formation of perovskite in a two-stage technology.

Let us consider the dynamics of the process of perovskite formation with variations of the MAI concentration in isopropanol. At low concentrations of the MAI solution, the appearance of a new perovskite phase in the form of small grains makes it possible for the continuation of the reaction at deeper levels of the lead iodide film. On the other hand, at high concentrations of the MAI solution, a perovskite film instantly forms on the surface of the second precursor film, making it difficult for MAI to diffuse to the underlying levels of lead iodide (direct reaction (2)). To confirm this mechanism, the authors [42] used various concentrations of MAI in isopropanol (0.038 M, 0.063 M, 0.1 M) in the formation of perovskite absorber. As expected earlier, the use of low concentrations of the MAI solution (0.038 M) leads to a more complete direct reaction and, as a result, to high conversion rates. Nevertheless, a small amount of unreacted lead iodide is found for this variant. The use of higher concentrations of MAI solution leads to a significant reduction of the conversion due to the presence of a large amount of lead iodide not involved in the formation of the perovskite phase. Thus, according to the experimentally confirmed Ostwald ripening model, fundamentally, due to the nature of the reactions of the precursors and the used solvents, it is impossible to have a complete conversion using the direct reaction. This means that the formation of an optimal morphology of the absorber with a high degree of coating of the substrate is very difficult.

The solution to these problems requires the finding of new approaches for a two-step perovskite technology for a planar cell configuration. Such approaches were soon found. First of all, they include special additives (including solvents) introduced into a solution of lead iodide to form amorphized films [43, 44]; solvent annealing and engineering [18, 19]; temperature variation of the solution and the substrate; the use of other lead compounds that do not contain halogens [45], etc.

Ahn et al. [46] proposed considering the two-step process from thermodynamic positions in order to identify the relationship between crystallite growth and reaction temperature for the mesoporous cell architecture. The expression for the Gibbs free energy taking into account the crystallization process is:

$$\Delta G_v = \frac{kT}{V_m} \ln \frac{C}{C_0(T)} \quad (3)$$

where ΔG_V is the change of Gibbs free energy per unit volume, C is the concentration of MAI, C_0 is the equilibrium MAI concentration, V_m is the volume of solute particle.

Taking into account the crystallization process, this equation is reduced to the form:

$$\Delta G_v = -a^3 \frac{kT}{V_m} \ln \frac{C}{C_0(T)} + 6a^2\sigma \quad (4)$$

where *a* is the length of the cube, σ is the average surface tension.

Differentiation of the equation by the size of cube-like crystal makes it possible to determine the critical values of the size ac and the Gibbs free energy ΔG_c:

$$a_c = \frac{4\sigma}{\frac{kT}{V_m} \ln \frac{C}{C_0(T)}} \quad (5)$$

$$\Delta G_C = \frac{32\sigma^2}{\left(\frac{kT}{V_m} \ln \frac{C}{C_0(T)}\right)^2} \quad (6)$$

$$Y(grain\ size) \sim a \sim \sqrt[3]{\frac{1}{n} \sim exp\left(\frac{\Delta G_C}{3kT}\right)} \quad (7)$$

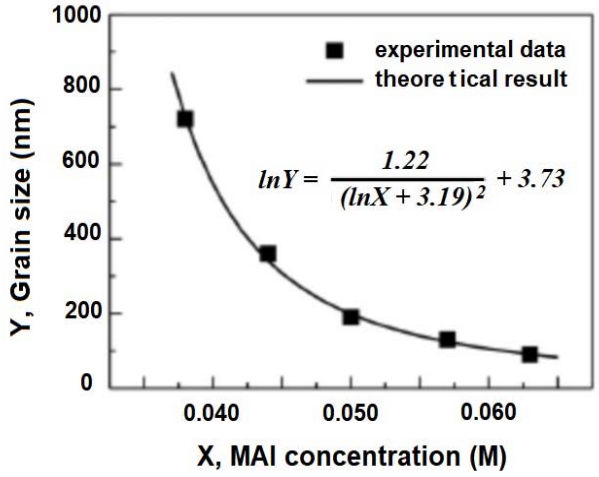

Fig. 2. Plot of theoretically derived $MAPbI_3$ grain size (Y) as a function of MAI concentration (X). The experimental data (filled square) were fit to a theoretical equation (Reproduced by permission of The Royal Society of Chemistry from [46]).

The free energy increases when the size of the growing crystal is less than the critical value and, conversely, decreases when the size is larger than the critical size.

Equation (7) can also provide information about the dependence of the crystal size on MAI concentration (Fig. 2). Such a conclusion completely coincides with the ones obtained in the Ostwald ripening model. It should be noted that this equation also relates the size of the growing crystal to temperature. For real cells formed using low concentrations of MAI (0.038 M) it has been experimentally confirmed that the size of the crystals is 700–800 nm, which has high PCE.

Summarizing the above, it can be argued that for a two-stage perovskite formation technology it is very important to control the sizes of the growing crystals by searching for optimally low concentrations of the MAI solution and temperature.

4. One-step technology of perovskite solar cells

Mixed perovskites due to the possibility increasing of the diffusion path length and the formation of crystallites with significant sizes of more than 1 μm (Cl-containing) and increasing the service life (Br-containing) attract the large attention of researchers [47–49]. Consider the peculiarities of the perovskite formation in the one-stage variant, which is carried out by spinning the solution of precursors (methylammonium iodide or chloride and lead iodide, or lead chloride). In the first case, methylammonium lead tri-iodide is formed, and a mixed-halide perovskite is formed in the second one. It has been proven that iodide perovskite is formed in both versions with no traces of the presence of chlorine atoms. However, it was found that the diffusion path length of photogenerated charge carriers is significantly higher (more than 1 micron) in the mixed perovskite than for perovskite iodide (100 nm). There are some attempts to explain the role of chlorine in providing such values (as a dopant, as a compound contributing to optimizing morphology, etc.). In our opinion, the Density Functional Theory, (DFT) calculations of defects in the perovskite structure should be considered the most acceptable, which indicates that the use of lead-containing precursor with no iodine atoms, they do not lead to the appearance of deep-lying levels in the forbidden zone responsible for the recombination processes. The standard perovskite is acceptable for the mesoporous cell architecture, whereas the mixed perovskite can be successfully used for the planar configuration of the cells.

The one-stage technology of perovskite production and optimization ways are widely presented in the literature, related to the refinement of the ratio of precursors, the choice of common solvent and solvent mixture, solution and substrate temperatures, to the influence of the humidity of the formed medium, to the introduction of special additives into the precursors solution, etc. Especially important is the colloidal chemical description of the precursor solution and the kinetics of the perovskite formation process corresponding to this state. Yan et al. [50] demonstrated the presence of Tyndall effect in the precursor solution, which points to the origin of these colloidal solutions. Dynamic light scattering on precursor solutions confirmed the presence of dispersion of the particle sizes from 10 nm to more than 1000 nm. This means that in addition to the dissolved lead iodide and MAI compounds, a number of coordination compounds are present in the precursor solution. Among them there can be various types of polyiodides of the anionic character up to the full octahedral structure.

Based on the initial preforms formed during the dissolution of precursors, the size of the final crystallites also has two types of size distribution, crystallites grown from polyiodides in the form of hexagonal disks with sizes up to 300 nm and from practically dissolved particles with sizes close to 10 nm.

For the solar cells with a standard ratio of precursors of CH_3NH_3I/PbI_2 of 1:1 conversion is 9% and 6% in the reverse and forward scans respectively. The authors attributed the low PCE and the observed hysteresis to the presence of unreacted lead iodide. A decrease or increase in the content of the organic precursor further reduces PCEs to less than 5% due to a large amount of free lead iodide and excess organic precursor (which is extracted at high temperatures and leads to the decomposition of perovskite), respectively. These problems were resolved by adding the methylammonium chloride to the precursors, which is released at lower temperatures and, as revealed earlier, this precursor at the dissolution stage tends to form polyiodide close to the octahedral structure.

Already when the ratio of precursors of $CH_3NH_3Cl/CH_3NH_3I/PbI_3$ is 0.5:1:1, the conversion rates are 10% and 9% in the forward and reverse directions, respectively. The authors determined that the ratio of 1:1.05:0.95 is optimal, the cells formed under these conditions and the thickness of the perovskite layer of 320 nm produce a conversion of 17%.

The above demonstrates how important the ratio and nature of the organic precursor in the reaction with the inorganic precursor in a colloidal solution is for a high-quality perovskite absorber to be achieved.

5. Influence of growth conditions on the form of nanocrystal nucleus

Among the problems of the growth of perovskite crystals under various conditions, a special place takes the determination of the possible shape of the formed nuclei. At present, this question has appeared in applications of technology using nanoparticles, in connection with the deviation of the shape of growing nanoparticles from spherical observed in a number of cases [51]. In addition to the obvious applied relevance of this problem, from a fundamental point of view, it is extremely important to identify the reasons for the appearance of such nonsphericity. Indeed, within the framework of the well-known Curie-Prigogine symmetry principle, the symmetry of the result of processes cannot be less than the symmetry of their causes [52]. In the above-mentioned problem of the growth of nanoparticles, this means that in isotropic solutions, the appearance of nonspherical nuclei is impossible, although the experiment indicates the opposite cases. To analyze the causes of this paradox, it is necessary, first of all, to take into account the fact that when formulating this principle, the condition of the proximity of systems to an equilibrium state and their macroscale dimensional characteristics was implicitly used, while deviation from these conditions, as will be shown below, removes the paradoxicality of the fact of coexistence nucleuses of various shapes.

Let us consider the process of growth of a nanoparticle in an isotropic medium. The rate of growth of the nucleus radius is described by the equation [53]:

$$\frac{dR}{dt} = a^3 j\alpha(R) = a^3 nv\alpha(R) \tag{8}$$

Here a^3 is the "size" of an atom deposited on the surface, j=nv is the flux of deposited atoms, n is their density at the surface of the nucleus, v is their thermal velocity. Let us assume that, as a result of fluctuations in the concentration n near the surface of the nucleus, on its surface (locally) a certain random build-up arises, the further evolution of which is determined by the competition between its diffuse spreading along the surface during the time

$$\tau_1 = R^2/D \tag{9}$$

where D is the surface diffusion coefficient, and it further increases as a result of the accommodation of particles falling on it from the solution (α(R) is the accommodation coefficient depending on the nucleus. Time of this accommodation process:

$$\tau_2 \approx \frac{1}{n^{1/3} v\alpha(R)} = \frac{n^{2/3}}{j\alpha(r)} \tag{10}$$

Further, the situation is as follows:

- under the regime $\tau_2>\tau_1$, diffusion spreading of the tubercle along the surface occurs;
- in the regime $\tau_2<\tau_1$, there is an accelerated growth of the tubercle.

To implement the latter mode, the condition of nonlinearity of accommodation is necessary: on a surface with a greater curvature 1/ρ, the value of α(1/ρ) must be greater:

$$\frac{d\alpha\left(1/\rho\right)}{d\left(1/\rho\right)} > 0 \tag{11}$$

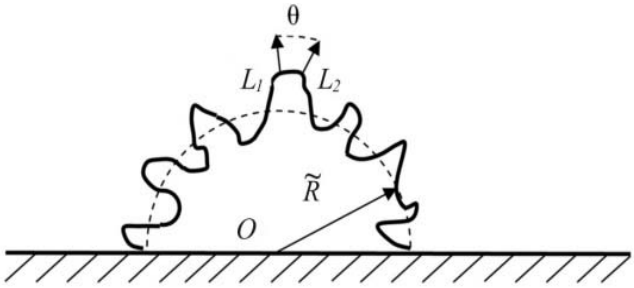

Fig. 3. Diagram of directions of neighboring Tamm orbitals (L_1 and L_2), differing by angle θ, hemispherical nanoparticle in case of its rough (fractal) surface [49, 50].

This is undoubtedly the case shown in Fig. 3 and discussed in [54] for a similar case of fractal nanocatalysis: an increase in the angle Θ between the surface Tamm orbitals, according to Coulson [55], enhances the reactivity, for example, to the capture of particles from the near-surface region. Then the condition $\tau_2 \approx \tau_1$ should divide the phase diagram (T;j) into two parts: at T>j the diffusion resorption is more effective, and the nucleus grows spherical; at T<j, the shape of the nucleus is non-spherical since fluctuations in atomic deposition prevail over resorption. Taking into account that the temperature T determines the rate of surface diffusion

$$D = D_0 \exp\left(-Q_q / kT\right) \tag{12}$$

then the equality $\tau_2 \approx \tau_1$ parametrically depends on the radius of the nucleus: the greater R, the easier the condition $\tau_2 < \tau_1$ is satisfied, i.e. the dashed line according to the inequality

$$\frac{n^{2/3}}{j\alpha(R)} < \frac{R^2}{D_0}\exp\left(Q_q / kT\right) \tag{13}$$

is placed below.

In addition to the conclusions about the ratio of T, R and j, we can say that an increase in the degree of supersaturation of the solution (large fluxes j) should lead to an increase in non-sphericity of the particle; the same effect should be observed with decreasing of temperature T.

6. Basic successes and important current problems

At present time, the registered conversion for perovskite solar cells is over 25.2%. Let us turn to a number of important factors underlying the achieved success [18–21, 50, 56].

The main strategy for solving the problem of effective coating of a perovskite film is to create conditions for an increase in the density of nucleating centers due to the acceleration of solvent evaporation.

The resolve of this problem took place thanks to comprehensive studies of the nature of solutions of perovskite precursors, namely, colloidal properties, that is, the formation of iodine-lead coordination complexes and their transformation into a perovskite structure during the spinning of solutions and subsequent heat treatment. Particular attention in this aspect deserves work on the formation of intermediate complexes, the interaction of Lewis acid and a base, among which are lead iodide and solvents dimethylformamide and dimethyl sulfoxide, respectively [56].

Another important problem is to provide favorable conditions for crystallization, the used solvents have high boiling points and low pressure of saturated vapors, and the residues of these solvents in the formed perovskite phase inevitably lead to their degradation. Some possible solution consists of the initiated studies on the choice of highly volatile solvents and the creation of favorable conditions for the formation of the required intermediate complexes by optimizing the ratio of precursors.

Significant advances have been made in the control of solvent evaporation after the spinning process, the use of an anti-solvent, the blowing of the surface of the forming film with gases, vacuum drying, and the method of high substrate temperatures. The introduction of additives to regulate the crystallization stage is also decisive in determining the optimal conditions for crystal growth in the range of 500–1000 nm, i.e. this morphology of the absorber significantly reduces the concentration of surface defect states. A large amount of research is associated with the optimization of interfaces, surface defects at the interface between crystals and their purposeful passivation, and the search in this connection for the choice of hole and electron conducting layers [57].

Despite the successes achieved, the commercialization of these devices is difficult due to the problems of instability and degradation in real operating conditions. Cell performance has undergone a significant leap since the first transducers were manufactured, from minutes to several thousand hours. At the same time, commercialization requires at least ten years of uptime guarantees. And this problem is the key one at the moment. It is noted that the intensity of research in this direction

is the highest; almost all important problems and ways to solve them are perfectly described in the review [58], which includes an analysis of many publications in recent years devoted to this section.

7. Introduction of solvent additives

One of the advantages of perovskite solar cells is the possibility of using solution technologies in the creation of these devices, which significantly reduces the cost of their production. In particular, a layer of a light-absorbing material, as well as auxiliary layers of selective semiconductors, can be applied from various solvents. At the moment, a large number of solvents used at different stages of assembly of perovskite solar cells are known, but the features of the interaction of solvent molecules with the light-absorbing material that affect its properties are not always known. This leads to a deterioration in the properties of light-absorbing materials in the solar cell and a decrease in the efficiency of the device as a whole.

In addition, the constant search for new organic and inorganic selective semiconductors requires the simultaneous selection of optimal solvents for their application on top of the hybrid perovskite layer without destroying the latter.

The main factor affecting the stability and efficiency of a photoelectric device is the stability of the crystal structure of the photoactive layer (perovskite). This depends mainly on the choice of materials, their composition and the method of obtaining a photoactive film. In addition, the adjustment of the stability of the structure can be provided by alloying elements and additives in the precursors. For example, solvent additives are usually used to control the crystal structure of perovskite.

As shown above, in order to optimize the morphology and crystal structure of the perovskite film, in addition to using different deposition methods, various solvent additives are used. According to the results [59], the introduction of a small number of solvent additives into solutions of perovskite precursors improves the crystal structure of the film and increases the performance characteristics of the entire device. The additives are introduced into the precursor solvents, which for lead halides and MAI are the polar aprotic solvents DMF, DMSO, GBL, and N-methyl-2-pyrrolidone (NMP). The organic solvents chlorobenzene, benzene, xylene, toluene, 2-propanol, and chloroform, despite their poor solubility, are also used in the preparation of solutions for organic conductive polymers and buffer layer materials.

Thus, the addition of acetonitrile (ACN) to the FAI/MABr/MACl precursor during the preparation of Cs-FA-MA perovskite using the sequential deposition method led to the fact that the surface defects on the perovskite film decreased and the grain size increased [60]. This modification of the film contributed to an increase in the PCI of the device to a value of 15.64% compared to the samples obtained without additives (13.06%). In addition, devices based on ACN additives showed more stable behavior in tests for resistance to atmospheric air, temperature and humidity. According to the results of a number of studies, the addition of DMF has a good effect on the morphology of the structure of $MAPbI_3$ perovskite films. By introducing methylammonium chloride (MACl) and a polar solvent as additional additives during two-stage sequential deposition, it was shown that DMF promotes easy penetration of MAI into the PbI_2 layer to form a dense perovskite film with a uniform morphology. Also, the addition of MAC1 induces $MAPbI_3$ to crystallize in the pure α-phase. The results of the study of the combined use of MAC1 and DMF demonstrate that a pure alpha-phase perovskite film with uniform morphology and a PCE of 19.02% and a VOC of up to 1.181 V. Oseni et al. [61] showed that in the two-stage processing method, the addition of DMSO to the solvent during the deposition of the first layer of PbI_2 led to the formation of smoother grains and uniform size with a reduced PbI_2 residue compared to films obtained using DMF.

Recent studies [62] in the preparation of hybrid perovskite ($CH_3NH_3PbI_3$) under conditions with high relative humidity (RH ~ 60%) of the atmosphere have shown that the use of a mixture of ethyl acetate and 4-tretbutylpyridine (tBP) as an anti-solvent contributes to the formation of a more homogeneous surface of perovskite with high hydrophobic ability. It is shown that the introduction of tBP in EA makes it possible to obtain a device with a PCE of 18.04% and maintain more than 80% of the initial efficiency for more than 180 days in conditions of high humidity. The addition of 1-chloro-naphthalene (CN) to the solvent in the preparation of the $CH_3NH_3PbI_3$ − film demonstrates a smooth and uniform film structure with fewer point holes and voids, and with a better surface coating than conventional films, but the degree of ultraviolet radiation absorption is lower, which indicates a non-uniform perovskite structure [63].

Bis (trifluoromethane) sulfonimidelithium salt (LiTFSI) is often used for p-doping, to increase the concentration of holes, in the Spiro-MeOTAD layer to achieve high PCE. Perovskite solar cells made of spiro (TFSI) 2 have shown improved stability in an inert atmosphere [64]. Thus, the modification of the perovskite structure by improving the film deposition technology and the introduction of various additives contribute to the improvement of the film morphology, to obtain a uniform and dense structure, which leads to an increase in the stability and efficiency of the device.

8. Surface engineering of perovskite nano-crystals to select the best ligands for filling surface traps with electrons

The authors of [65] carried out surface engineering of perovskite nano-crystals to select the best ligands for filling traps with electrons. They obtained laboratory samples of perovskite nanocrystals suspensions. Metal halide perovskite nano-crystals were synthesized by colloid ligand assisted reprecipitation (LARP) method.

For the synthesis of nanocrystals by the LARP method, a solution of perovskite CH_3NH_3Br (MAPBr) was prepared. 11.2 mg of CH_3NH_3Br and 36.7 mg of $PbBr_2$ were dissolved in 1 ml of dimethyl formamide (DMF). Then 200 μl of oleic acid and varying amounts of octylamine/oleylamine were added to the solution: 15, 30, and 60 μl of octylamine in the first series of samples; 15, 30, and 60 μl of oleylamine in the second series. Afterwards, 100 μl of perovskite solution with ligands was added to 3 ml of toluene with vigorous stirring. The solution acquired a green color and a greenish glow when illuminated with ultraviolet light.

Next, the nanocrystals synthesized by the LARP method [66] were washed with different amounts of a toluene/acetonitrile (1:1) mixture (600 and 800 μL) and centrifuged at 9000 rpm for 2 min. The particles were dispersed in toluene. The glass substrates were UV treated for 15 min. This method helped to obtain a uniform film. The nanocrystal film was covered by poly-methyl methacrylate (PMMA) to increase the stability of the layer when working outdoors. The washing suspensions of nanocrystals with a mixture of toluene/acetonitrile improve their optical properties. For studying the structural properties of MAPBr, perovskite nanocrystals were synthesized by the LARP, as mentioned earlier method. The structural peculiarities and morphology of MAPBr nanocrystals were studied using a Crossbeam 540 scanning electron microscope (SEM) (Carl Zeiss), JEM-1400 Plus (JEOL) transmission electron microscope (TEM) for samples deposited on an optically polished crystalline silicon wafer and a gold grid with carbon-coated, respectively.

Figure 4 shows SEM images of MAPBr nanocrystals with average sizes of 130 (a), 50 (b) and 6 (c) nm. Figure 6 shows the corresponding histograms of the size distribution of nanocrystals (bars) approximated by lognormal functions (lines).

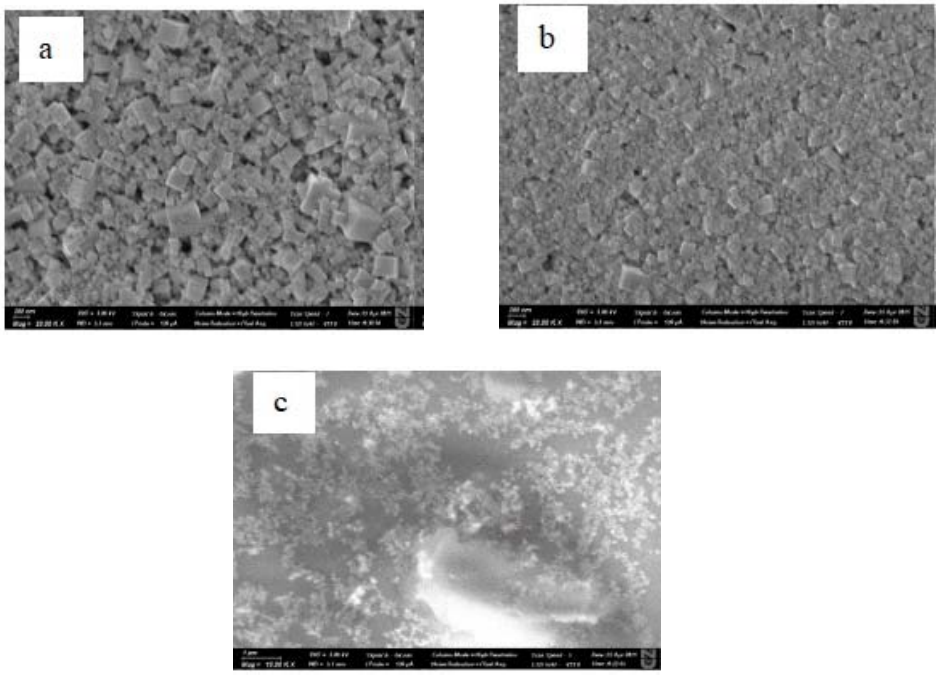

Fig. 4. SEM images of MAPBr nanocrystals with average sizes of 130 (a), 50 (b), and 6 nm (c).

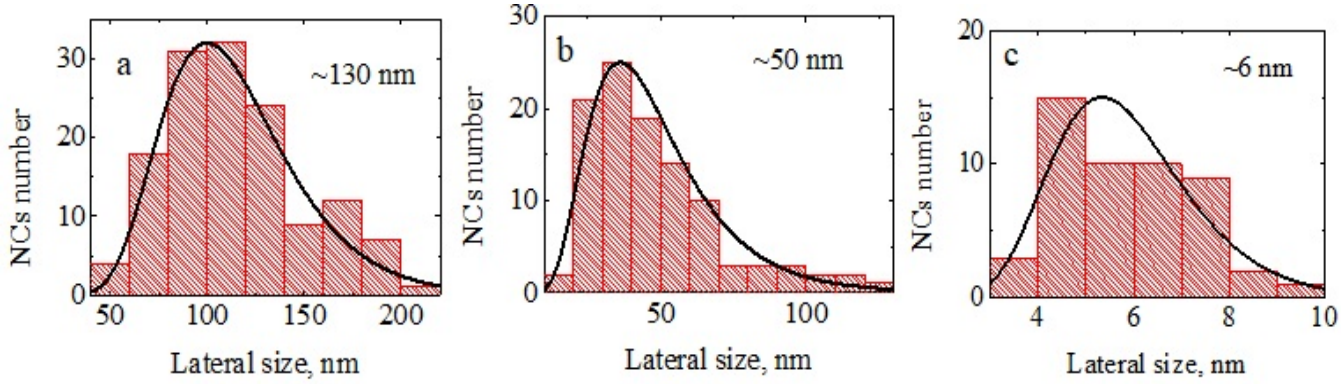

Fig. 5. Size distribution histograms of MAPBr nanocrystals (bars) with average sizes of 130 (a), 50 (b), and 6 nm (c) approximated by lognormal functions (lines).

According to SEM data (Fig. 4), the synthesized MAPBr nano-crystals have cubic shape with average transverse dimensions of 6 ± 1.4, 50 ± 2 and 130 ± 30 nm (Fig. 5) for samples prepared with different amounts of ligand (octylamine). It is noticeable that the nano-crystals thickness can be much smaller than their transverse dimensions.

Some important theoretical aspects of processes in perovskite-based solar cells are presented in [67, 68].

9. Conclusions

1. It was shown that current technological advances and developments require the use of reliable sources of energy that guarantee the sustainability of our near future.

2. The concepts presented in this paper on the features of the formation of a perovskite layer in one- and two-stage technologies using a number of progressive approaches (introduction of additives, crosslinking of perovskite crystallites, regulation of the nucleation and crystal growth by adding anti-solvents, temperature annealing and annealing with solvents, etc.) open up broad prospects for improving the optoelectronic characteristics of a perovskite absorber and the conversion characteristics of solar cells based on them.

3. An analysis of literature data showed that the most promising is a synthesis of perovskite nanocrystals by the method of colloidal reprecipitation with ligand-assisted reprecipitation (LARP).

4. The use of benzyl alcohol in addition to the octylamine ligand and oleic acid promotes the formation of perovskite nanocrystals with long-term stability: the nanocrystals retain their photoluminescence intensity for more than three weeks.

Acknowledgments

This research has been funded by the Science Committee of the Ministry of Education and Science of the Republic of Kazakhstan (Grant № AP08855457).

References

[1]. M. Graetzel, *Nat. Mater.* 13 (2014) 838–842. DOI: 10.1038/nmat4065

[2]. N.-G. Park, *Mater. Today* 18 (2015) 65–72. DOI: 10.1016/j.mattod.2014.07.007

[3]. M.A. Green, A. Ho-Baillie, H.J. Snaith, *Nat. Photonics* 8 (2014) 506–514. DOI: 10.1038/nphoton.2014.134

[4]. N.R. Ashurov, B.L. Oksengendler, S.Sh. Rashidova, A.A. Zakhidov, *Appl. Sol. Energy* 52 (2016) 5–15. DOI: 10.3103/S0003701X16010023

[5]. N.R. Ashurov, B.L. Oksengendler, S.E. Maksimov, S.Sh. Rashidova, A.R. Ishteev, D.S. Saranin, I.N. Burmistrov, D.V. Kuznetsov, A.A. Zakhidov, *Mod. Electron. Mater.* 3 (2017) 1–25. DOI: 10.1016/ j.moem.2017.05.001

[6]. M. Rini, R. Tobey, N. Dean, J. Itatani, Y. Tomioka, Y. Tokura, R.W. Schoenlein, A. Cavalleri, *Nature* 449 (2007) 72–74. DOI: 10.1038/nature06119

[7]. C. Li, X. Lu, W. Ding, L. Feng, Y. Gao, Zguo, *Acta Cryst.* B64 (2008) 702–707. DOI: 10.1107/S0108768108032734

[8]. G. Yar-Mukhamedova, M. Ved, N. Sakhnenko, M. Koziar, *Appl. Surf. Sci.* 421 (2017) 68–76. DOI: 10.1016/j.apsusc.2017.01.196

[9]. H.S. Kim, C.R. Lee, J.H. Im, K.B. Lee, T. Moehl, A. Marchioro, S.J. Moon, R. Hamphry-Baker, J.H. Yum, J.E. Moser, M. Graetzel, N.G. Park, *Sci. Rep.* 2 (2012) 591. DOI: 10.1038/srep00591

[10]. G.Sh. Yar-Mukhamedova, A.M. Darisheva, E.

Sh. Yar-Mukhamedov, *Mater. Sci.* 54 (2019) 907–912. DOI: 10.1007/ s11003-019-00279-y
[11]. Y.F. Chiang, J.Y. Jeng, M.H. Lee, S.R. Peng, P. Chen, T.F. Guo, T.C. Wen, Y.J. Hsu, C.M. Hsu, *Phys. Chem. Chem. Phys.* 16 (2014) 6033–6040. DOI: 10.1039/C4CP00298A
[12]. A. Kemelzhanova, G. Zhamanbayeva, A. Zakhidov, V. Kurmangaliyeva, E. Temirgaliyeva. Proc. Paper, 20th International Multidisciplinary Scientific GeoConference SGEM 2020. DOI: 10.5593/sgem2020/4.1/s17.015
[13]. G.E. Eperon, V.M. Burlakov, P. Docampo, A. Goriely, H.J. Snaith, *Adv. Func. Mater.* 24 (2014) 151–157. DOI: 10.1002/adfm.201302090
[14]. Z. Xiao, C. Bi, Y. Shao, Q. Dong, Q. Wang, Y. Gao, J. Huang, *Energy Environ. Sci.* 7 (2014) 2619–2623. DOI: 10.1039/C4EE01138D
[15]. G. Yar-Mukhamedova, *Mater. Sci.* 36 (2020) 598–601. DOI: 10.1023/A:1011382609756
[16]. H. Hu, D. Wang, Y. Zhou, J. Zhang, S. Lv, Sh. Pang, X. Chen, Zh. Liu, N.P. Padture, G. Cui, *RSC Adv.* 4 (2014) 28964–28967. DOI:10.1039/C4RA03820G
[17]. M.R. Leyden, L.K. Ono, S.R. Raga, Y. Kato, Sh. Wang, Y. Qi, *J. Mater. Chem. A* 2 (2014) 18742–18745. DOI:10.1039/c4ta04385e
[18]. Z. Xiao, Q. Dong, C. Bi, Y. Shao, Y. Juan, J. Huang, *Adv. Mater.* 26 (2014) 6503–6509. DOI: 10.1002/adma.201401685
[19]. N.J. Jeon, J.H. Noh, Y.Ch. Kim, W.S. Yang, S. Ryu, S. Seok, *Nat. Mater.* 13 (2014) 897–903. DOI: 10.1038/nmat4014
[20]. M. Xiao, F. Huang, W. Huang, Y.Dkhissi, Y.Zhu, J Etheridge, A. Gray-Weale, U. Bach, Y.-B. Cheng, L. Spiccia, *Angew. Chem. Int. Edit.* 53 (2014) 9898–9903. DOI: 10.1002/anie.201405334
[21]. K.O. Brinkmann, J. He, F. Schubert, J. Malerczyk, C. Kreusel, F. van gen Hassend, S. Weber, J. Song, J. Qu, Th. Riedl, *ACS Appl. Mater. Interfaces* 11 (2019) 40172–40179. DOI: 10.1021/acsami.9b15867
[22]. A. Ng, Zh. Ren, H. Hu, P.W.K. Fong, Q. Shen, S.H. Cheung, P. Qin, J.-W. Lee, A.B. Djurišic, S.K. So, G. Li, Y. Yang, Ch. Surya, *Adv. Mater.* 30 (2018) 1804402. DOI: 10.1002/adma.201804402
[23]. A. Kojima, K. Teshima, Y. Shirai, T. Miyasaka, *J. Am. Chem. Soc.* 131 (2009) 6050–6051. DOI: 10.1021/ ja809598r
[24]. NREL Best Research-Cell Effciencies, https://www.nrel.gov/pv/assets/images/effciency-chart.png (accessed: April 2019)
[25]. X. Li, W. Zhang, X. Guo, C. Lu, J. Wei, J. Fang, *Science* 375 (2022) 434–437 DOI: 10.1126/science.abl567
[26]. W.S. Yang, J.H. Noh, N.J. Jeon, Y.C. Kim, S. Ryu, J. Seo, S.I. Seok, *Science* 348 (2015) 1234–1237. DOI: 10.1126/science.aaa9272
[27]. D. Bi, W. Tress, M. Ibrahim Dar, P. Gao, J. Luo, C. Renevier, K. Schenk, A. Abate, F. Giordano, J.-P. Correa Baena, J.-D. Decoppet, S.M. Zakeeruddin, M.K. Nazeeruddin, M. Grätzel, A. Hagfeldt, *Sci. Adv.* 2 (2016). DOI: 10.1126/sciadv.1501170
[28]. H.P. Zhou, Q. Chen, G. Li, S. Luo, T.-Bing Song, H.-S. Duan, Z. Hong, J. You, Y. Liu, Y. Yang, *Science* 345 (2014) 542–546. DOI: 10.1126/science.1254050
[29]. M. Liu, M.B. Johnston, H.J. Snait, *Nature* 501 (2013) 395–398. DOI: 10.1038/nature12509
[30]. P. Docampo, J.M. Ball, M. Darwich, G.E. Eperon, H.J. Snaith, *Nat. Commun.* 4 (2013) 2761. DOI: 10.1038/ncomms3761
[31]. W. Nie, H. Tsai, R. Asadpour, J.-C. Blancon, A.J. Neukirch, G. Gupta, J.J. Crochet, M. Chhowalla, S. Tretiak, M.A. Alam, H.-L. Wang, A.D. Mohite, *Science* 347 (2015) 522–525. DOI: 10.1126/science.aaa0472
[32]. C.-G. Wu, C.-H. Chiang, Z.-L. Tseng, Md.K. Nazeruddin, A. Hagfeldt, M. Graetzel, *Energy Environ. Sci.* 8 (2015) 2725–2733. DOI: 10.1039/C5EE00645G
[33]. W. Chen, Y. Wu, Y. Yue, J. Liu, W. Zhang, X. Yang, H. Chen, E. Bi, I. Ashraful, M. Graetzel, L. Han, *Science* 350 (2015) 944–948. DOI: 10.1126/science.aad1015
[34]. K.-Ch. Wang, P.-Sh. Shen, M.-H. Li, Sh. Chen, M.-W. Lin, P. Chen, T.-F. Guo, *ACS Appl. Mater. Interfaces* 6 (2014) 11851–11858. DOI: 10.1021/am503610u
[35]. K.-C. Wang, K.-Y. Jeng, P.-S. Shen, Y.-C. Chang, E. Wei-Guang Diau, C.-H. Tsai, T.-Y. Chao, H.-C. Hsu, P.-Y. Lin, P. Chen, T.-F. Guo, T.-C. Wen, *Sci. Rep.* 4 (2014) 4756. DOI: 10.1038/srep04756
[36]. J.Y. Jeng, K.C. Chen, T.Y. Chiang, P.Y. Lin, T.D. Tsai, Y.C. Chang, T.F. Guo, PChen, T.C. Wen, Y.J. Hsu, *Adv. Mater.* 26 (2014) 4107–4113. DOI: 10.1002/adma.201306217
[37]. Z. Zhu, Y. Bai, T. Zhang, Z. Liu, X. Long, Z. Wei, Z. Wang, L. Zhang, J. Wang, F Yan, S. Yang, *Angew. Chem. Int. Edit.* 53 (2014) 12571–12575. DOI: 10.1002/anie.201405176
[38]. W. Chen, Y. Wu, J.Liu, Ch. Qin, X. Yang, A. Islam, Y.-B. Cheng, L. Han, *Energy Environ. Sci.* 8 (2015) 629–640. DOI: 10.1039/C4EE02833C
[39]. J.H. Park, J. Seo, S. Park, S.S. Shin, Y.C. Kim et al., *Adv. Mater.* 27 (2015) 4013–4019. DOI: 10.1002/adma.201500523
[40]. J.W. Jung, C.C. Chueh, A.K. Jen, *Adv. Mater.* 27 (2015) 7874–7880. DOI: 10.1002/adma.201503298
[41]. J.-H. Im, H.-S. Kim, N.-G. Park, *APL Mater.* 2

(2014) 081510. DOI: 10.1063/1.4891275
[42]. S.-Y. Kim, H.J. Jo, Sh.-J. Sung, D.-H. Kim, *APL Mater*. 4 (2016) 100901. DOI: 10.1063/1.4963841
[43]. F. Wang, H. Yu, H. Xu, N. Zhao, *Adv. Funct. Mater*. 27 (2015) 1120–1126. DOI: 10.1002/adfm.201404007
[44]. W. Zhang, S. Pathak, N. Sakai, T. Stergiopoulos, P.K. Nayak, et al., *Nat. Commun.* 6 (2015) 10030. DOI:10.1038/ncomms10030
[45]. F.K. Aldibaja, L. Badia, E. Mas-Marza, R.S. Sanchez, E.M. Barea, I. Mora-Sera, *J. Mater. Chem. A* 17 (2015) 7–16. DOI: 10.1039/C4TA06198E
[46]. N. Ahn, S.M. Kang, J.-W. Lee, M. Choi, N.-G. Park, *J. Mater. Chem. A* 3 (2015) 19901–19906. DOI: 10.1039/C5TA03990H
[47]. F. Di Giacomo, S. Razza, F. Matteocci, A. D'Epifanio, S. Licoccia, T.M. Brown, A. Di Carlo, *J. Power Sources* 251 (2014) 152–156. DOI: 10.1016/j.jpowsour.2013.11.053
[48]. G.E. Eperon, S.D. Stranks, C. Menelaou, M.B. Johnston, L.M. Herz, H.J. Snaith, *Energy Environ. Sci.* 7 (2014) 982–988. DOI: 10.1039/C3EE43822H
[49]. N. Pellet, P. Gao, G. Gregori, T.-Y. Yang, M.K. Nazeeruddin, J. Maier, M. Gratzel, *Angew. Chem. Int. Ed.* 53 (2014) 3151–3157. DOI: 10.1002/ anie.201309361
[50]. K. Yan, M. Long, T. Zang, Z. Wei, H. Chen, S. Yang, J. Xu, *J. Am. Chem. Soc.* 137 (2015) 4460–4468. DOI: 10.1021/jacs.5b00321
[51]. M. Isaiev, G. Mussabek, P. Lishchuk, P. Lishchuk, K. Dubyk et al. *Nanomaterials* 12 (2022) 708. DOI: 10.3390/nano12040708
[52]. G. Yar-Mukhamedova, M. Ved', I. Yermolenko, N. Sakhnenko, A. Karakurkchi, A. Kemelzhanova, *Eurasian Chem.-Technol. J.* 22 (2020) 19–25. DOI: 10.18321/ectj926
[53]. H.C. Wang, Z. Bao, H.Y. Tsai, A.C. Tang, R.S. Liu, *Small* 14 (2018) 1702433. DOI: 10.1002/smll.201702433
[54]. B.L. Oksengendler, V.N. Nikiforov, S.E. Maksimov, *Dokl. Phys.* 62 (2017) 281–283. DOI: 10.1134/S1028335817060039
[55]. P. Wang, Y. Wu, B. Cai, Q. Ma, X. Zheng, W. H. Zhang, *Adv. Funct. Mater.* (2019) 1807661. DOI: 10.1002/adfm.201807661
[56]. N. Ahn,D.-Y.Son, I.-H. Jang, S.M. Kang, M. Choi, N.-G. Park, *J. Amer. Chem. Soc.* 137 (2015) 8696–8699. DOI: 10.1021/jacs.5b04930
[57]. T. Salim, S. Sun, Y. Abe, A.Krishna, A.C. Grimsdale, Y.M. Lam, *J. Mater. Chem. A* 3 (2015) 8943–8969. DOI: 10.1039/c4ta05226a
[58]. T.A. Berhe, W.-N. Su, Ch.-H. Chen, Ch.-J. Pan, J.-H. Chen, H.-M. Chen, M-Ch. Tsai, L.-Y. Chen, A.A. Dubale, B.-J. Hwang, *Energy Environ. Sci.* 9 (2016) 323–356. DOI: 10.1039/c5ee02733k
[59]. F. Huang, M. Li, P. Siffalovic, G. Cao, J. Tian, *Energy Environ. Sci.* 12 (2019) 518–549. DOI: 10.1039/C8EE03025A
[60]. G. Yar-Mukhamedova M. Ved', N. Sakhnenko, A. Karakurkchi, I. Yermolenko, *Adv. Mater. Sci. Eng*. 2021, 5511127. DOI: 10.1155/2021/5511127
[61]. S.O. Oseni, G.T. Mola, *J. Phys. Chem. Solids* 130 (2019) 120–126. DOI: 10.1016/j.jpcs.2019.02.015
[62]. A. Zakhidov, G. Zhamanbayeva, G. Yar-Mukhamedova, *Complex Use of Mineral Resources* 4 (2021) 19–24. DOI: 10.31643/2021/6445.36
[63]. M. Isaiev, G. Mussabek, P. Lishchuk, K. Dubyk, et al., *Nanomaterials* 12 (2022) 708. DOI: 10.3390/nano12040708
[64]. K. Sekerbayev, G. Mussabek, Y. Shabdan, Y. Taurbayev, *Eurasian Chem.-Technol. J.* 23 (2021) 89–93. DOI: 10.18321/ectj1078
[65]. I. Levchuk, P. Herre, M. Brandl, A. Osvet, R. Hock, W. Peukert, P. Schweizer, E. Spiecker, M. Batentschuk, C.J. Brabec, *Chem. Commun.* 53 (2017) 244–247. DOI: 10.1039/C6CC09266G
[66]. A. Kirakosyan, J. Kim, S.W. Lee, I. Swathi, S.G. Yoon, J. Choi, *Cryst. Growth Des.* 17 (2017) 794–799. DOI: 10.1021/acs.cgd.6b01648
[67]. N.N. Turaeva, B.L. Oksengendler, *Appl. Solar Energy* 54 (2018) 318–321. DOI: 10.3103/S0003701X18050195
[68]. B.L. Oksengendler, N.R. Ashurov, S.E. Maksimov, M.I. Akhmedov, I.N. Nurgaliev, *Appl. Solar Energy* 53 (2017) 326–333. DOI: 10.3103/S0003701X17040119